J. Fluid Mech. (1984), *vol.* 141, *pp.* 1–25
Printed in Great Britain

Temperature-field structure within atmospheric buoyant thermals

By R. G. BATT, R. A. BIGONI† AND D. J. ROWLAND
TRW Space and Defense Systems Group, Redondo Beach, CA 90278

(Received 22 June 1981 and in revised form 14 October 1983)

Using stationary rakes of hot-wire anemometer probes, a series of temperature measurements have been conducted within rising buoyant thermals created by detonation of large-diameter gas-filled balloons. These atmospheric detonation simulation tests were performed at the SANDIA Laboratories Aerial Cable Test Facility, Kirtland AFB, during the late fall of 1973. All measurements were performed after pressure equilibrium ($t > 1$ s) but prior to completion of the toroid formation process and within the time required ($t > 4$ s) for the fireball to rise one diameter.

Based on an extensive processing of measured data for two detonation events, unique results describing the mean flow field and turbulent structure statistics for the early-time large-scale buoyant thermal have been determined. Final results include: mean-velocity and temperature data; temperature and temperature gradient intensities; space, auto- and 'eddy-lifetime' correlation scales; power-spectral densities; probability density distributions and approximate microscale data.

The present temperature data illustrate that the early-time rising fireball is characterized by a highly intermittent irregular top or cap, a constant (high-) temperature core and a thermal wake exhibiting a linear decay in mean temperature. Mean convection velocities for the fireball wake were measured to be approximately twice as large as fireball cap velocities (13.1 m/s). Maximum fireball temperatures (1100 °C) were in good agreement with peak brightness-temperature data determined from an independent IR measurements experiment. Core leading-edge mean-temperature gradients compare favourably with predictions (10 °C/cm) whereas trailing-edge gradients (0.4 °C/cm) are smaller than predicted results (3 °C/cm).

Normalized temperature intensities at the fireball top and within the thermal wake were substantial (≈ 0.6) in contrast with quiescent fireball core levels (0.1). Moving-frame autocorrelation times ('eddy lifetimes', 0.17 ± 0.04 s) were approximately four times larger than measured autocorrelation times. This result illustrates that the early-time fireball eddy structure is highly persistent, a finding which tends to substantiate those radar models for large-scale fireballs which postulate relatively slow 'smearing' of early-time electron density gradients. Wake integral scales, determined from vertical space correlation data, were approximately 5% of the fireball mean radius. Probability density distributions for the fireball thermal wake were 'spiky' in nature, with some evidence of bimodal behaviour, and slightly skewed to the negative side of their normalized values. Normalized spectra data, in general, follow a $-\frac{5}{3}$ falloff behaviour for several decades in spectral power. The noted large 'spread' in the inertial subrange is consistent with measured turbulence Reynolds numbers (2000) and with the large-scale fully developed turbulent structure for the GEST fireballs ($Re_D = 3 \times 10^7$). Wake microscale data, estimated from temperature

† Present address: Mission Research Corporation, 735 State Street, Santa Barbara, CA 93102.

and temperature-gradient intensity data and the isotropic turbulence assumption, varied from 2 to 4 cm and were in favourable agreement with predicted microscale magnitudes.

1. Introduction

The rising buoyant thermal has been a subject of interest to investigators for many years. Small-scale laboratory experiments have been performed to determine overall size/rise characteristics as well as mass-entrainment behaviour (e.g. Scorer 1957; Woodward 1959). These measured data have been complemented by optical measurements of high-temperature fireballs from atmospheric nuclear events (Taylor 1950). Considerable success has also been achieved in performing small-scale buoyant thermal measurements of turbulent structure statistics (Lin, Tsang & Wang 1972; Tsang 1974) and mean-density profiles (Mantrom & Haig 1974).

Related to these experimental studies of the buoyant thermal is the development of sophisticated numerical codes which predict overall buoyant thermal dynamics including the behaviour of the low-altitude nuclear fireball. The large radar backscattering produced by these latter intense high-temperature thermals give rise to the familiar radar clutter and communications blackout phenomena. Code-development activities seek to predict not only the behaviour of weapon systems in a nuclear environment but also the nature and extent of electromagnetic wave attenuation/scatter caused by the fireball's turbulent high-temperature electron-rich flow field (Knapp & Schwartz 1975). Important in validating these predictive capabilities, as well as in clarifying the source for radar clutter and blackout, is the use of initial-condition data quantifying the relationship between the structure of the turbulent temperature field and the gross motion of the early-time large-scale fireball. Although some success has been realized in measuring turbulent structure statistics for small-scale buoyant thermals, there still exists a lack of detailed turbulence data for the early-time large-scale fireball.

In response to this need for additional buoyant thermal turbulence data, a series of multiprobe fast-response temperature measurements have been conducted within large-scale rising fireballs through use of stationary rakes of hot-wire anemometer probes. Such measurements were performed within atmospheric buoyant thermals created by detonation of large-diameter gas-filled balloons under the Defense Nuclear Agency's balloon-detonation test program (GEST). Reduced results as presented herein are intended to provide a set of data for use in supporting development and evaluation of analytical models for buoyant thermals as well as for clarifying radar backscatter phenomena for the nuclear fireball. All measurements were performed after pressure equilibrium ($t > 1$ s) but prior to completion of the toroid formation process and within the time required ($t > 4$ s) for the fireball to rise one diameter. The present reduced temperature data therefore provide unique initial-condition results quantifying the temperature-field structure for the early-time large-scale fireball.

2. Technical approach

The Gas Explosive Simulation Technique (GEST) program (Bigoni & Matuska 1973), was conducted under Defense Nuclear Agency (DNA) sponsorship by the Air Force Weapons Laboratory (AFWL). This experimental program involved a series of atmospheric detonation experiments using 10 m balloons suspended above ground

($h \approx 39.6$ m) and filled with a near-stoichiometric mixture of methane and oxygen gases. These nuclear-fireball simulation tests were performed at the SANDIA Laboratories Aerial Cable Test Facility, Kirtland AFB, which is located at an altitude of 1890 m corresponding to an atmospheric pressure of 82.7 kPa. An overhead cable, at approximately 18.3 m above detonation centre was used during the tests to support the required thermal instrumentation which consisted of stationary rakes of calibrated hot-wire anemometer probes. This steel-wire cable (2.54 cm diameter) was installed under a previous field-test program and was lowered to ground level to facilitate attachment of the probe strut systems and related sensor cables.

2.1. *Test schedule*

Although multiple-probe temperature measurements were attempted on five detonation events (table 1), adequate fireball data return was achieved only on events 3 and 4. The inability to obtain measured results for the other events was brought about by a combination of wind-induced fireball drift as well as early-time failure of hot-wire sensors due to balloon debris.

During early checkout experiments with small-diameter balloons, it was found that a methane/oxygen gas mixture (near-stoichiometric) provided superior detonation performance as compared with a mixture of carbon monoxide/oxygen. By mixing methane (CH_4) and oxygen (O_2) in the approximate ratio of 1 part to 2 parts respectively by volume and inflating the mylar balloons to 10 m in diameter, an energy yield equivalent to approximately 1500 pounds of TNT was achieved. The computed yields for the detonations are noted in table 1. Detonation of the explosive mixture was initiated by three RP-1 detonators positioned at the centre of each balloon. Tracer-gas seeding of the detonation cloud was accomplished by wrapping the detonators with plastic containers filled with aluminium oxide powder. All mylar balloons were constructed of three-mil mylar coated on both sides with a 5000 Å thick layer of aluminium.

2.2. *Test-site configuration*

An elevation view of the test-site configuration for events 3 and 4 is given in figure 1 and an assembly drawing of the probe mounting strut is shown in figure 2. Note that, with the vertical leg of the strut's triangular framework positioned at approximately 9.1 m from the fireball centreline, the two instrumented legs measure data both in the azimuthal and radial directions. In addition, the use of seven and three probes, spaced 0.46 m apart on the azimuthal and radial legs respectively, provided results spanning the expected scale dimensions. All wire sensors were aligned orthogonal to the vertical plane through the overhead cable (figure 2). Cable/balloon separation distances as well as the number of activated temperature probes are noted in table 1.

2.3. *Hot-wire anemometry technique*

Depending on the particular application, the hot-wire anemometer measurement procedure involves operating a small wire sensor in either the constant-temperature (T_w) or constant-current (i_w) mode (Kovasznay 1954; Corrsin 1949). Although the constant-current sensor (resistance thermometer) provides a voltage output signal proportional to temperature through resistivity calibration data, the constant-temperature anemometer determines, as will be shown below, not only local temperature data but also mean-velocity results for the rising GEST fireballs. In order to realize the beneficial aspects of measuring temperatures directly while at the same time providing a means for determining local fireball velocities, an instrumentation

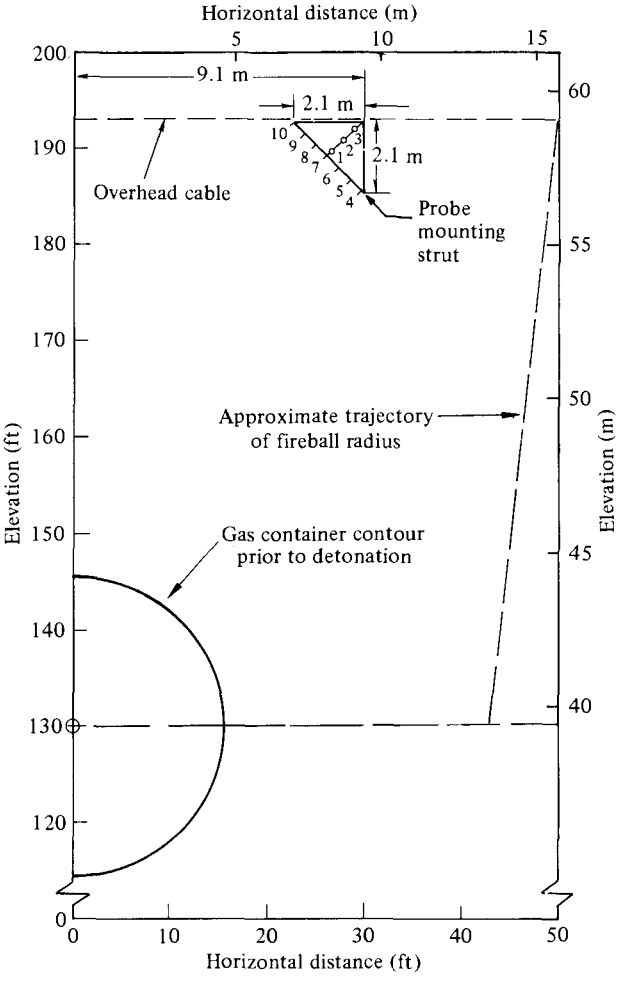

FIGURE 1. Side view of test-site layout.

matrix was selected which included a mix of both constant-current ($i_w \approx 3.7$ mA) and constant-temperature (700–800 °C) anemometer channels.

2.3.1. *Probe configuration*

All probe sensors for events 3 and 4 of the GEST Program were either 63.5 μm platinum–iridium or 50 μm platinum–tungsten wire sensors ($l \approx 0.13$ cm). All wires were silver-soldered to the probe stem needle supports for the two types of high-temperature probes used in the investigation (radial or azimuthal) (figure 2). The frequency response for the constant-current sensors (channels 2 and 7) was limited by wire thermal lag to approximately 1 kHz, whereas the hot-wire probes operating in the constant-temperature mode (channels 1, 3–6 and 8–10) were frequency compensated by the anemometer's feedback bridge to provide a 5 kHz response.

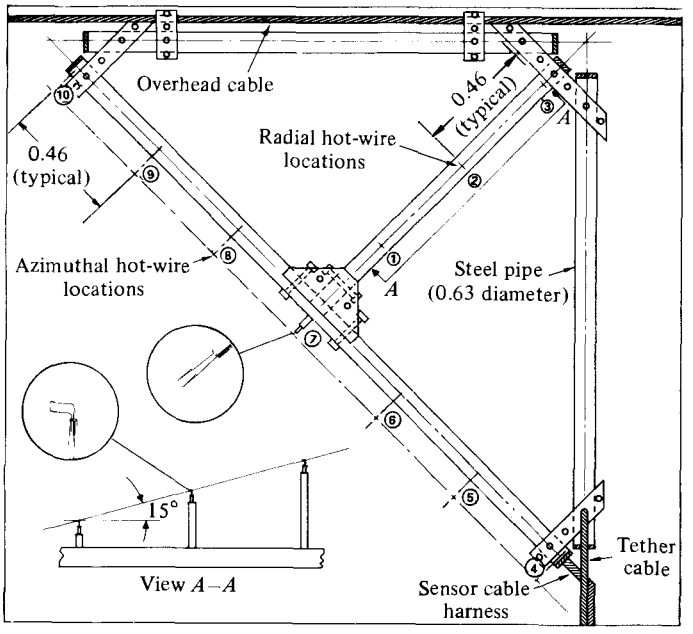

FIGURE 2. Probe strut configuration (m).

2.3.2. *Data reduction*

To reduce the measured bridge-voltage signal for a constant-temperature anemometer to flow-field temperature data, the heat-transfer relation for a wire sensor is used. This is given by

$$\left(\frac{e_w}{R_w}\right)_M = \left(\frac{e_w^2}{R_w}\right)_0 + Nu\,\pi lk(T_w - T), \tag{1}$$

where e_w, R_w and T_w represent the voltage, resistance and temperature respectively for the wire sensor; Nu and k correspond to the Nusselt number and conductivity respectively; l is the wire length and T is the local gas temperature. The subscripts M and 0 refer to measured and end-loss conditions respectively. Substantial calibration results relating Nusselt number Nu and Reynolds number Re have been reported by Bradshaw (1971), and the empirical correlation presented therein (as modified to account for an effective reference temperature),

$$Nu = 0.21 + 0.46 Re^{0.45}, \tag{2}$$

has been used to process the present set of data.

The first term on the right-hand-side of (1) represents the heat lost to the probe tips (end-loss effect), and it was assumed to remain constant during the short measurement times involved in the fireball-temperature experiments. This power-loss term was measured in the laboratory and verified in the field under no-flow (ambient) conditions. Additionally, sensor operating temperatures and sensor nominal diameters and lengths were also determined during laboratory calibrations.

To enhance data resolution, a second flow calibration was performed for each sensor. Use was made, in this latter calibration, of the result that all fireball-temperature data were obtained after the GEST fireball achieved pressure equilibrium ($t > 1$), at which time the wire Reynolds number became a function only of

Event	Test date	Time (h)	Balloon height (m)	Strut range (m)	T_{amb} (°C)	Wind		Yield (GJ)	Sensor survival	Validated channels	Fireball data return	
						Direction	Speed (m/s)				Fidu time span (s)	Total channels
1	28 Nov. 73	0940	46	12	−1	330°	1.5	2.86	7	1–10	—	0
2	30 Nov. 73	0930	43	9	+1	Gusting	1.1	2.93	0	1, 2, 5, 7–9, 11	—	0
3	11 Dec. 73	0925	40	9	+5	Gusting	1.1	3.00	9	1–10	1.7–3.8	10
4	13 Dec. 73	0800	40	9	+5	135°	1.1	2.72	10	1–3, 5–11	1.4–3.6	10
5	19 Jan. 74	1000	40	15	+4	60°	2.6	1.45/3.20	13	5–8, 10–12	1.6–4.4	5

TABLE 1. Test-matrix summary; balloon diameter, 10 m; cable height, 60 m; sensors activated 12

temperature and velocity. Also, as will be discussed further in §3.3, the trailing wakes of the GEST fireballs contained vertically moving pockets of unmixed ambient air which were identifiable by their quiescent nature. Since the temperature and velocity for these ambient 'eddies' were known, i.e. $T = T_{\text{ambient}}$ and $u = u_{\text{convection}}$ (from vertical cross-correlation statistics, §3.6.1), sensor calibration constants could be verified by matching the sensor output signal to the local velocity/temperature conditions (equation (1)). Thus by flow-calibrating a given wire sensor for ambient air conditions just prior to detonation as well as by use of motion statistics for unmixed ambient fluid contained within the fireball wake, a unique pair of calibration constants was arrived at for each sensor. Prior to final processing of the fireball data, a determination was made of the local velocity time history (§3.3) for each event by back-calculating convection velocities for all detectable ambient eddies. Once the fireball's velocity/time dependence had been specified, solving (1) for temperature data was accomplished in an iterative manner using flow-calibrated channel constants and the noted mean-velocity data.

To carry out the required data-reduction calculations, special-purpose temperature-conversion programs were written to calculate single-channel mean and statistical properties as well as cross-correlation statistics between any pair of selected channels. Since the primary data base occurred at frequencies less than 1 kHz and in order to avoid data-alaising difficulties, a conservative Nyquist or folding frequency of 2 kHz was established. The corresponding sample rate was 4000 samples/s, and all statistically processed results reported herein were based on this digitized rate.

3. Experimental results

The test schedule for the GEST balloon-detonation program is presented in table 1. In addition to a listing of performance dates, detonation yields, atmospheric test conditions and number of activated temperature channels, table 1 also specifies balloon/strut separation distances, validated channel results, sensor survival performance and a summary of fireball data return. Specific probe location/orientation details have been presented in §2. As noted in §2.1, fireball data return was limited and/or not achieved on several events due to wind-induced fireball drift (event 1), substantial debris-induced sensor failure (event 2) or signal-to-noise difficulties (event 5). Thus processing and reduction of measured results to determine temperatures and turbulent statistics for the GEST fireballs have concentrated herein on results for events 3 and 4. For raw data results, sensor-bridge operational characteristics and additional discussion on events 1, 2 and 5 the reader is referred to Batt (1976).

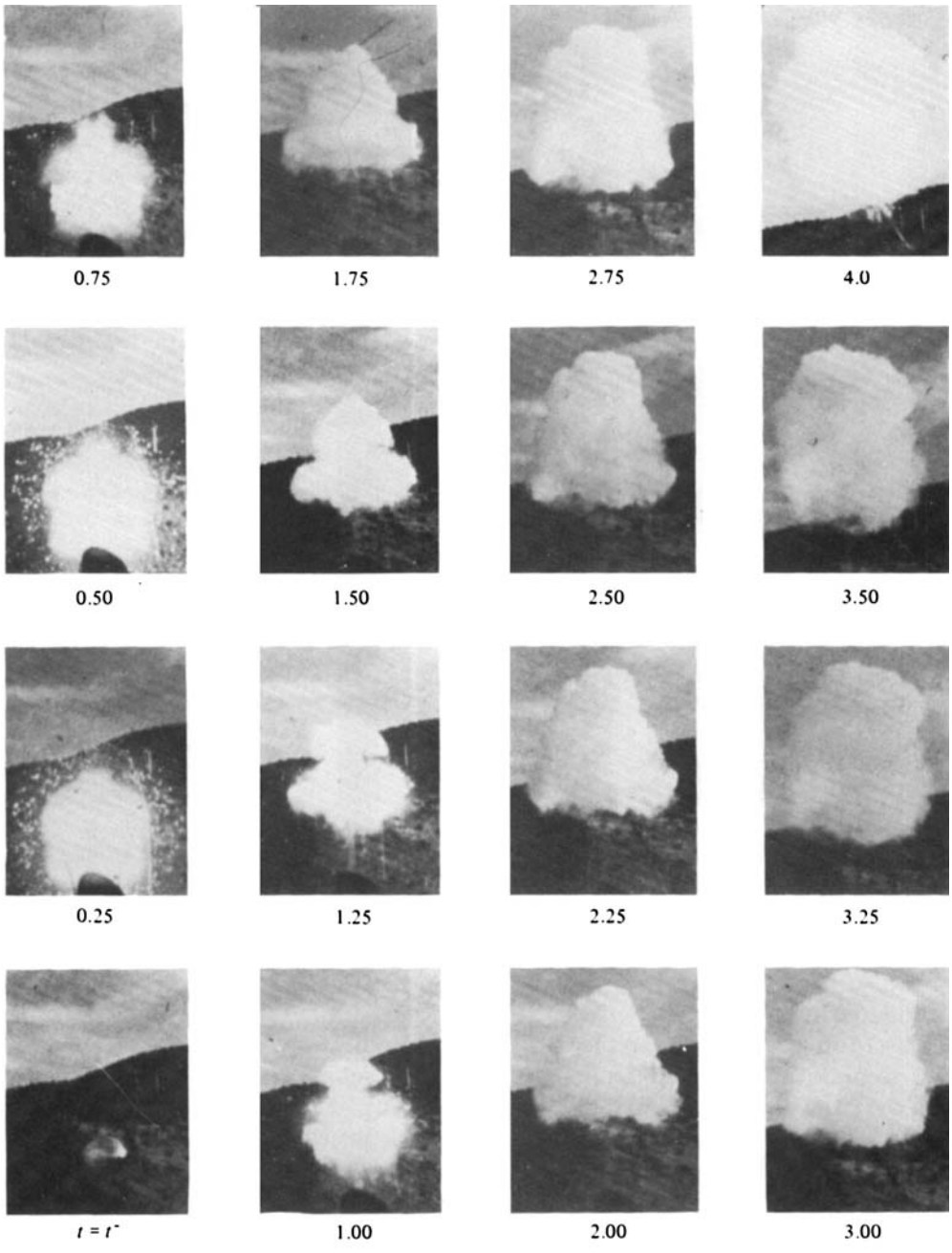

FIGURE 3. Event 3 fireball.

3.1. *GEST size/rise data*

Prior to discussing the details of measured temperature results for events 3 and 4, it is appropriate to assess general performance characteristics for the rising GEST fireballs. To this end reference is made to the side-view motion-picture results obtained by AFWL as shown in figures 3 and 4. These sequential film clips were prepared from 16 mm colour films (400 frames/s) taken by Fastex cameras located approximately 1000 ft from GZ. Note that sensor-detected fireball leading/trailing-

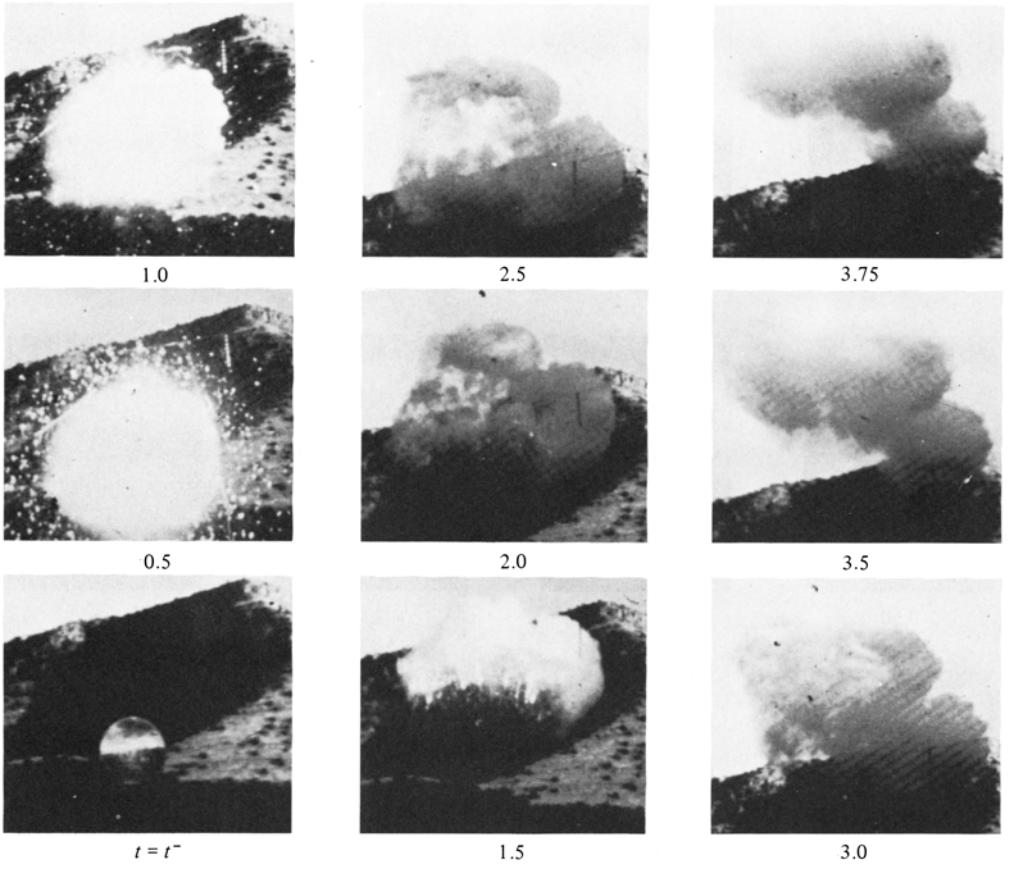

FIGURE 4. Event 4 fireball.

edge times were 1.7/3.8 s and 1.4/3.6 s for events 3 and 4 respectively (table 1). In addition to the fireball cloud, also visible in figures 3 and 4 are the overhead cable, the sensor cable harness, the main probe strut, and a 15 ft (4.6 m) black-and-white scaling marker.

This 15 ft marker was used by AFWL as a calibration 'scale' to determine the size/rise data presented in figure 5 (Bigoni & Matsuka 1974). These data illustrate that the fireballs for events 3 and 4 rose vertically at a velocity of approximately 13.1 m/s and were nearly 33 m in diameter during the time GEST temperature data were measured. Corresponding fireball Reynolds numbers based on these diameter and velocity data and ambient conditions were of the order of 3×10^7. From motion-picture films taken by cameras positioned directly below balloon centre, vortex formation became evident at approximately 4–5 s after detonation. These photographic results also illustrate that the main probe strut for the temperature task was positioned at approximately the half-maximum radius location (figure 1). The resulting data correspond to a vertical slice through the rising fireball, thus providing multiprobe temperature measurements for the fireball top, central core and trailing wake. Evident in figures 3 and 4 are the fast-rising centre 'cap', vertical motion around the fireball perimeter, and the early-time turbulent structure for the GEST fireballs. Intermittent 'pockets' of ambient air are also observed to be entrained by the turbulent fireball and subsequently to pass through the temperature-probe locations.

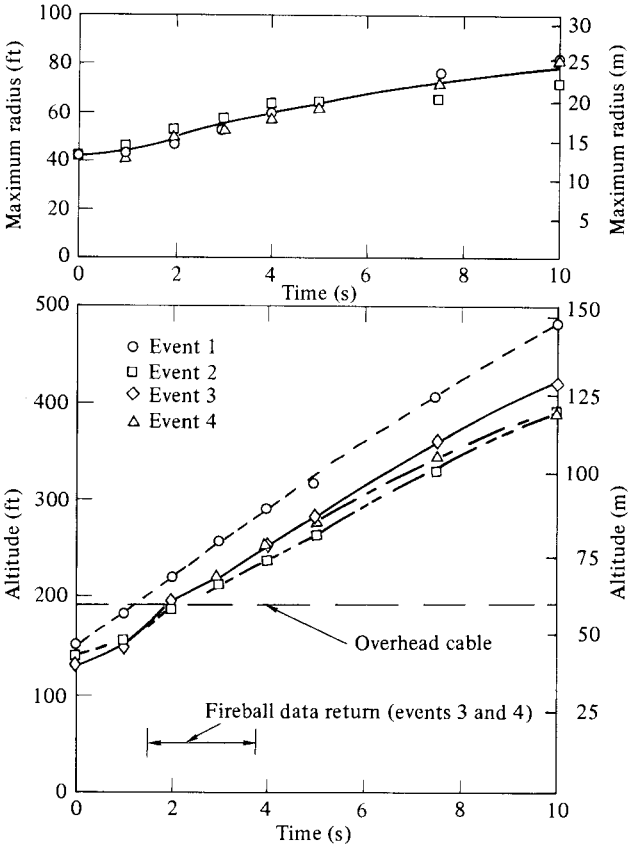

FIGURE 5. Trajectory data for GEST fireballs – optical measurements (Bigoni & Matuska 1974).

3.2. *Raw-data time-trace histories*

Typical raw-data time-trace histories for event 4 are shown in figure 6. Response of the heat transfer gauge (constant-temperature sensors, channels 1 and 3) to shock-front motion is seen to be distinct from the fireball response. The noted difference is a direct result of the heat-loss equation for the constant-temperature hot wire, which for a rising GEST fireball is given approximately by

$$e_w^2 \approx (CT + u^{\frac{1}{2}})(T_w - T). \tag{3}$$

This form for the reduced heat-transfer equation illustrates that, in order to maintain a constant wire temperature, the bridge feedback power must increase with increasing velocity when flow temperature changes are negligible. Similarly, when velocity changes are small but substantial temperature increases occur, as within the fireball, feedback power is reduced. Although the bridge power signal represents the combined effects of both the velocity and temperature field within the fireball, its dependence on velocity is relatively small because of the velocity's square-root behaviour.

3.3. *Mean-velocity data*

In scoping out the original instrumentation matrix for GEST, consideration was given to the need to measure local flow velocities as well as to optimize the use of available equipment. Thus the final test configuration consisted of a mix of 'direct' and

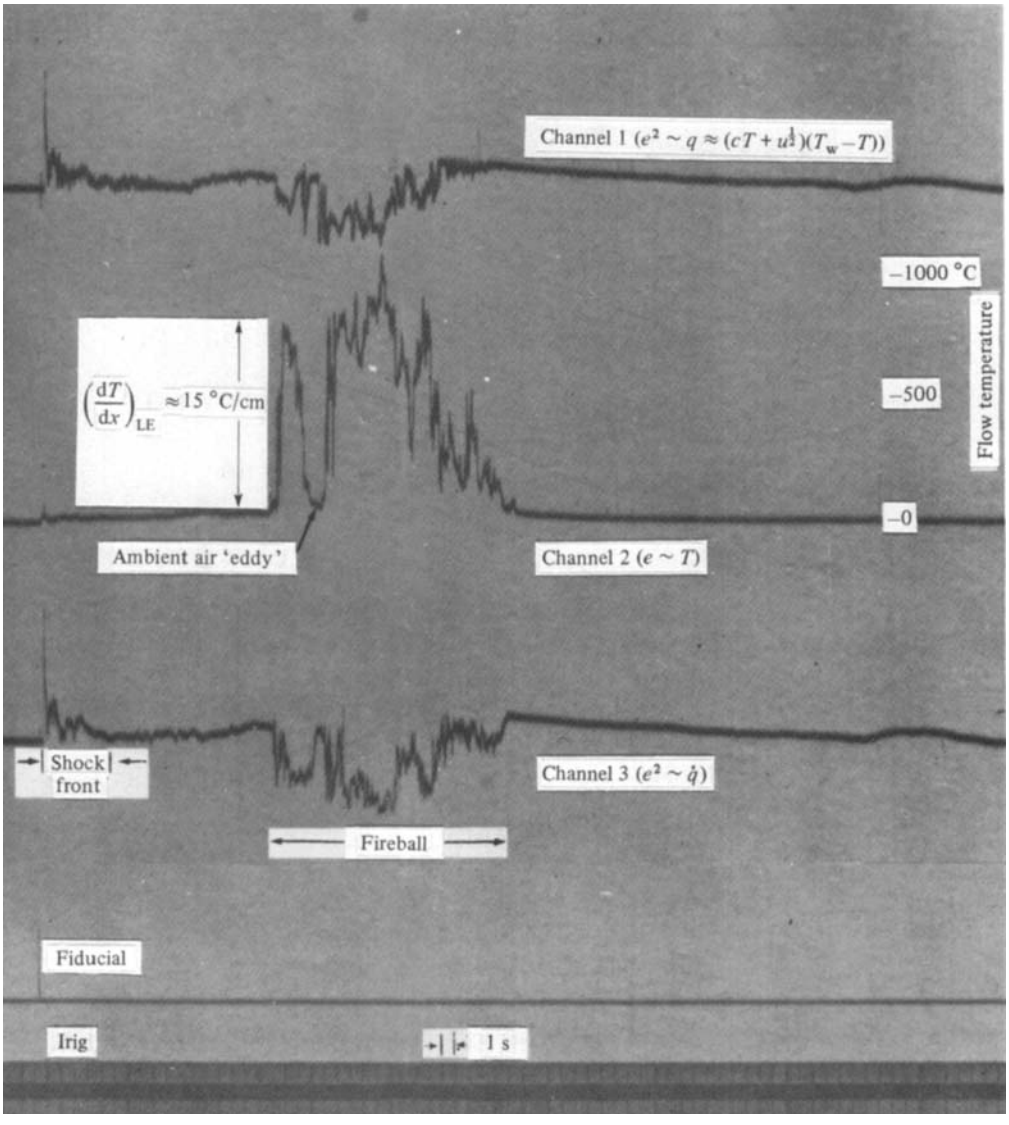

FIGURE 6. Raw-data oscillograph records – event 4.

'derived' temperature-measurement channels. Both types of measurements employed hot-wire anemometry techniques in either the constant-current mode (direct) or constant-temperature mode (derived) (§2.3). The 'derived' anemometry procedure permits a determination to be made of the mean velocity field by 'backing-out' local velocities from measured heat-transfer data associated with the motion of ambient air. Since unmixed ambient fluid is identifiable by its quiescent nature, local velocity data can be determined directly from the sensor heat-transfer equation (§2.3.2). In this manner, reduced velocity results for events 3 and 4 have been 'measured' and are shown as open-symbol data in figures 7 (*a*, *b*) respectively. Shown also on figures 7 (*a*, *b*) are local convection velocities as determined by 'eddy' time delays between vertically adjacent channels.

To assist in evaluating these velocity data, annotation entries for the mean rise

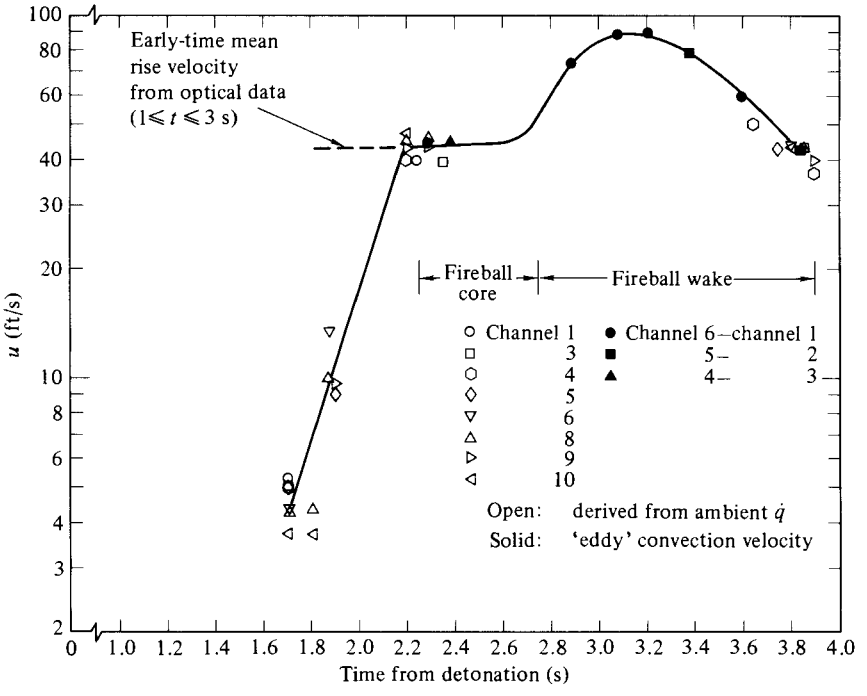

(*a*)

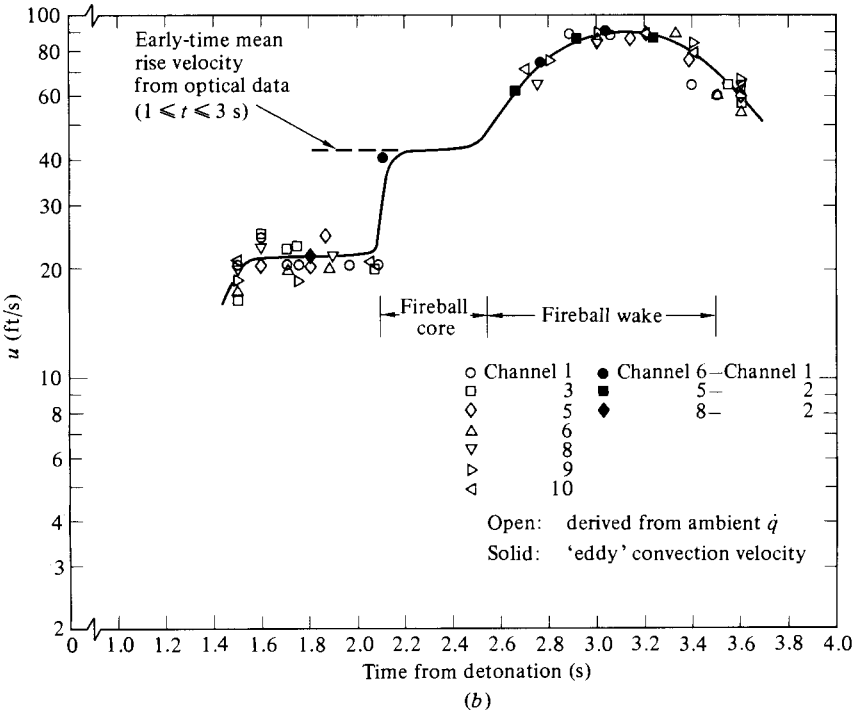

(*b*)

FIGURE 7. Mean-velocity data: (*a*) event 3; (*b*) event 4.

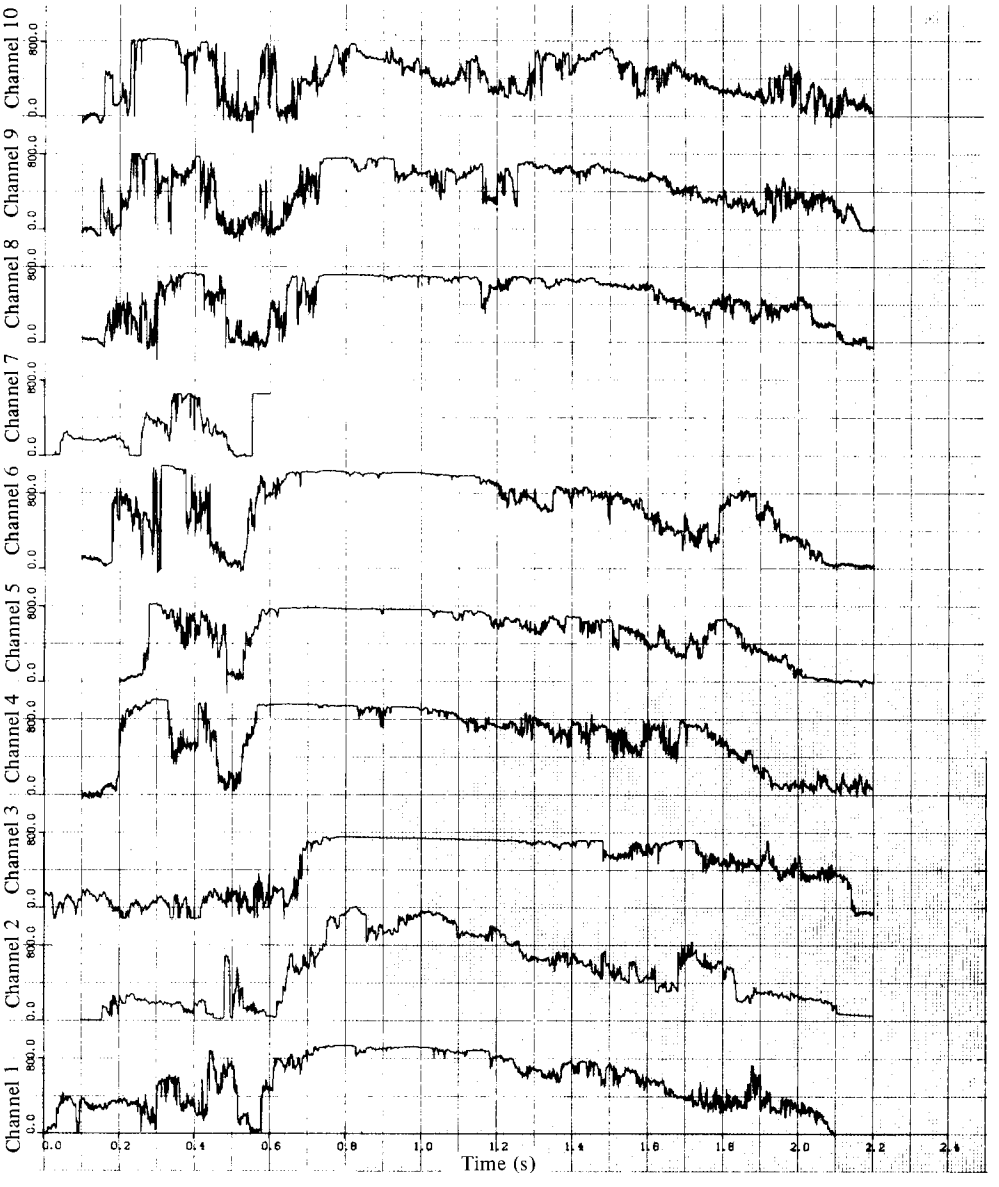

(*a*)

FIGURE 8(*a*). For caption see facing page.

velocity derived from optical data (§3.1) as well as relative locations for the fireball core and thermal wake (based on mean-temperature results) are also shown on figures 7*a*, *b*). The noted data, especially the event 3 results, provide evidence that the fireball leading edge is moving vertically at a velocity comparable to the optically derived mean rise velocity (13.1 m/s). On the other hand, velocity results for the fireball thermal wake illustrate that velocities as high as twice the core velocities were experienced. Such a result compares favourably, however, with the maximum flow velocities for Hill's spherical-vortex model (Lamb 1932), which predicts maximum velocities 2.5 times larger than the mean rise velocity.

As a final point relative to the figure 7 results, it should be noted that the velocities

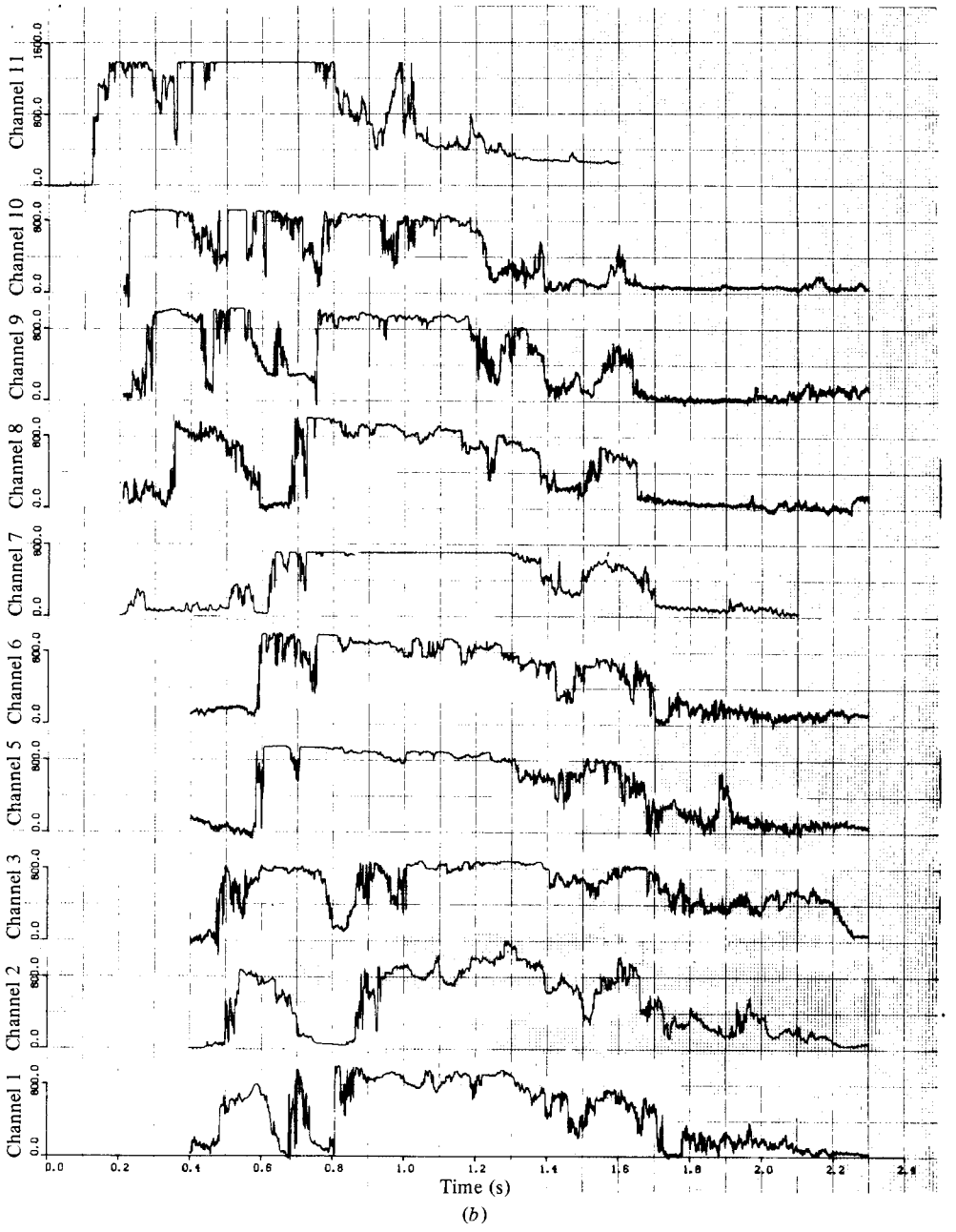

(*b*)

FIGURE 8. Digitized fireball-temperature data: (*a*) event 3 ($t_{\text{fidu}} = -1.7$ s); (*b*) event 4 ($t_{\text{fidu}} = -1.3$ s).

at the top of the fireball for events 3 and 4 are significantly different. This contrasting behaviour, however, is consistent when it is recognized that portions of the fireball top/cap for event 4 were initially moving radially (horizontally) at substantial speeds (see e.g. figure 4). This radial motion behaviour was determined after reviewing high-speed motion-picture results for GEST fireballs as well as radially correlating 'cap' turbulence data for channels 8 and 2 of event 4.

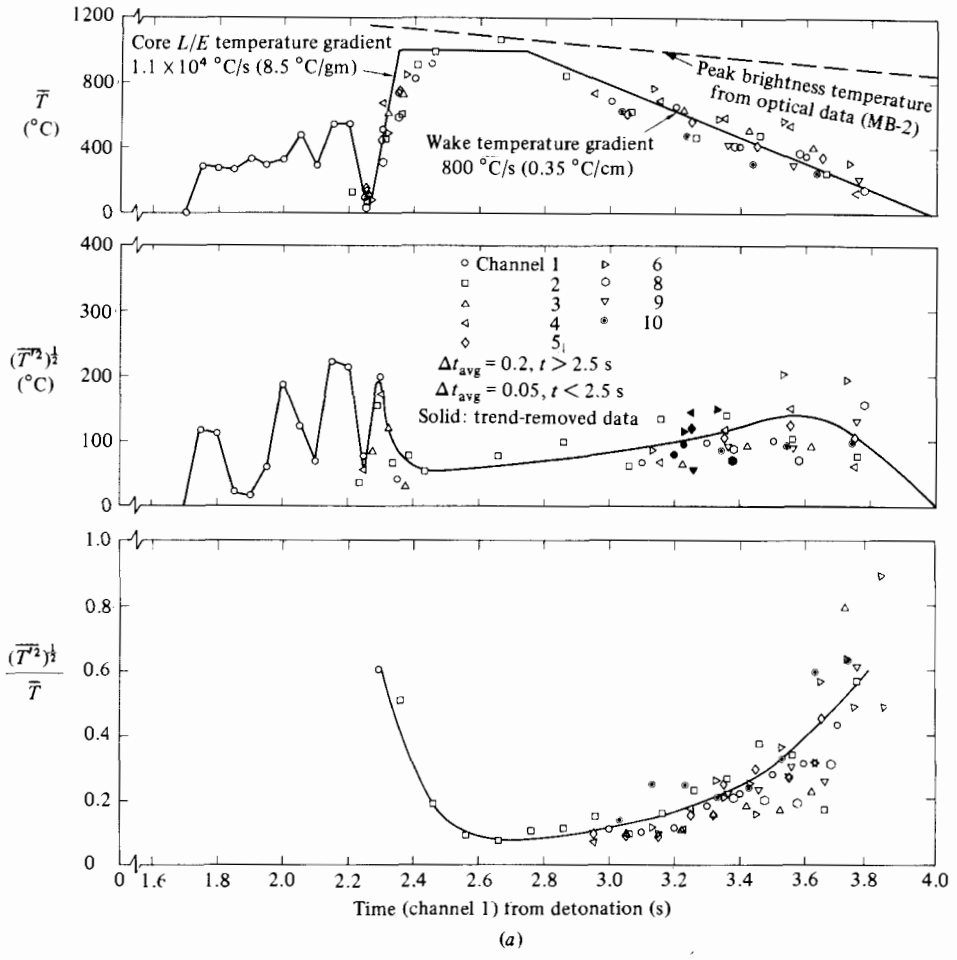

FIGURE 9(*a*). For caption see facing page.

3.4. *Temperature time-trace histories*

From the digitized raw data, reduced temperature results for events 3 and 4 are presented in figures 8(*a*, *b*). Sensor locations for the noted data are shown in the test configuration layout drawing of figure 2. In figure 8(*a*, *b*) channels 2 and 7 correspond to resistance-thermometer measurements, wherein the bridge-output signal is proportional to temperature, while all other channels represent reduced temperatures determined from sensor heat-transfer data as 'measured' buy anemometer bridge voltages.

In statistically processing the present non-stationary turbulence data, it was important initially to assess the presence of repeatable (deterministic ensemble averages) and/or locally stationary (trend phenomena) data characteristics (Bendat & Piersol 1971; Blackman & Tukey 1958). In reviewing the present temperature-history data and in spite of some signal overrange difficulties, a relatively consistent model for the GEST fireball does indeed become apparent. To a first approximation the noted data illustrate that the early-time rising fireball is characterized by a highly intermittent irregular fireball top or cap, a relatively constant high-temperature core and a thermal wake exhibiting (approximately) a linear decay in mean temperature. Not only are temperature fluctuations near the fireball 'top' and 'bottom' of the same

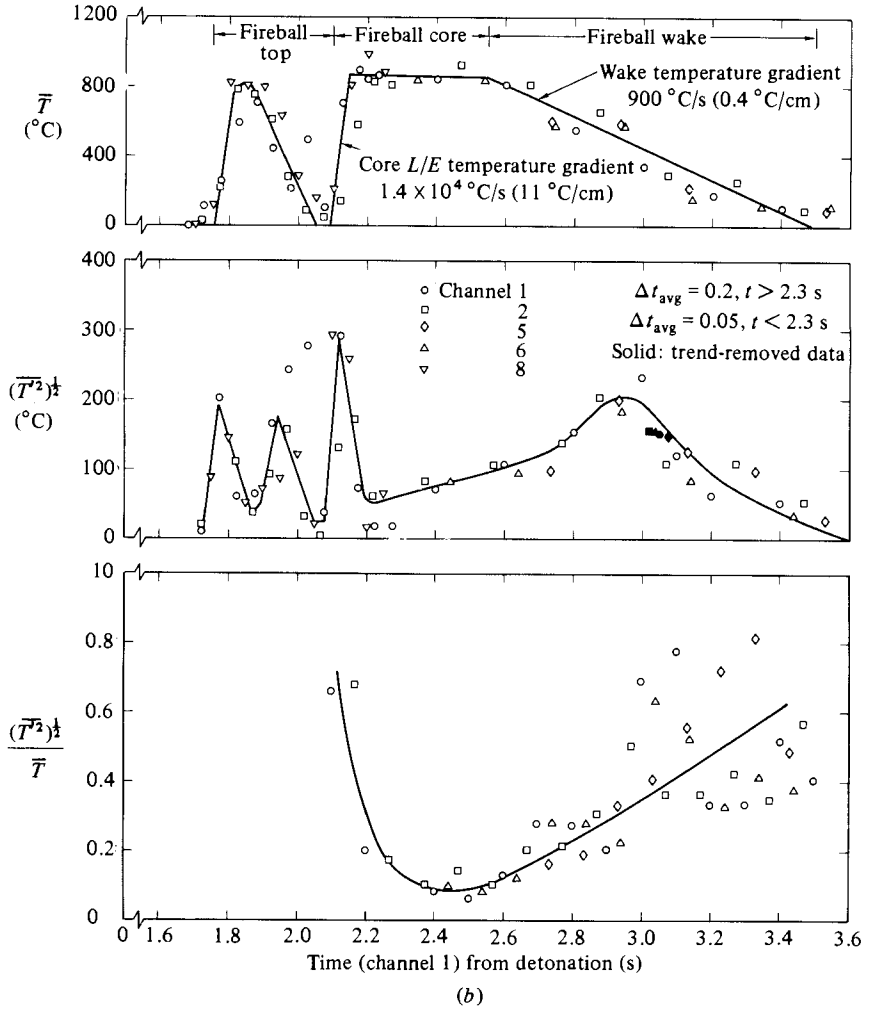

(*b*)

FIGURE 9. Time-averaged temperature data: (*a*) event 3; (*b*) event 4.

order as the mean temperature, but these fluctuations, as well as temperatures and temperature gradients, are all higher at the leading edge of the fireball compared with corresponding values at the trailing edge. Note, for example, the rather 'sudden' growth in temperature/intensity at the top of the fireball as compared to the gradual decay at the bottom. Leading edges of 'hot' eddies and the fireball core are in general characterized by steep temperature gradients relative to trailing edges which contain relatively shallow gradients. Hot fluid motion at the fireball top consists of large-scale structure in combination with random pockets of intense turbulent activity. The presence of ambient air eddies (pockets) embedded/entrained within the fireball flow field is evident in the time-trace data of figure 8, a finding consistent with results from the GEST photographic coverage. This first-order thermal 'picture' of a rising fireball agrees favourably with available laboratory data for buoyant thermals (e.g. figure 6 of Lin *et al.* 1972).

3.5. *Time-averaged mean and r.m.s. temperature data*

Summarized results for mean and r.m.s. temperature data for events 3 and 4 are presented in figures 9(*a*, *b*) respectively. The core and wake data shown represent

reduced results as validated for only those channels/times where flow turbulence is established (i.e. non-intermittent) and where signal saturation difficulties are not present. Only limited data are presented for fireball top conditions, since such measured data are highly irregular and intermittent. All data have been shifted in time such that core leading edges are aligned with the core leading edge for channel 1. This time adjustment corresponds to the assumption that spatial changes in fireball characteristics occur 'slowly' relative to the fireball rise velocity. For the data of figures 9(*a*, *b*), averaging interval times of 0.2 and 0.05 s were used for the core/wake and top respectively. All data, as shown, are plotted as a function of midinterval times. The noted time intervals were chosen after a study of random non-stationary effects was completed showing that such times were sufficient to provide approximate invariance of averaged temperature data with interval size.

Examination of the results of figures 9(*a*, *b*) provides further confirmation that the GEST fireballs do indeed exhibit consistent and reproducible behaviour. From the mean-temperature data in particular, it becomes apparent that the approximate locations for the fireball top, core and wake can be clearly designated. The peak brightness temperature data from optical measurements for event 2 (Bigoni & Matuska 1974) are also shown on figure 9(*a*), and favourable comparison is evident. Since the detonation yields for events 2 and 3 were similar (≈ 3.00 J), the agreement noted provides a consistency check between two separate experiments. In addition, such a field-test comparison substantiates the temperature measurement accuracy of the IR scanning technique and further justifies its use in measuring peak-temperature data on other large-scale detonation events. Some decrease in temperature is evident between events 3 and 4 and this result is consistent with the fact that the detonation yield for event 4 was about 10% lower than the yield for event 3 (table 1). Trailing-edge mean-temperature gradients for both events are approximately 0.4 °C/cm, whereas core leading-edge gradients are 8.5 °C/cm and 11 °C/cm for events 3 and 4 respectively. These mean-gradient results contrast with instantaneous gradient data, which were measured to be as high as 300 °C/cm. Although event 3 leading-edge gradients are low relative to predictions (11 °C/cm; Bigoni & Matsuka 1974), the event 4 data are seen to compare favourably. Predicted temperatures, on the other hand, compare poorly with the present temperature data in terms of maximum temperature (2000 °C) and trailing-edge gradients (≈ 3 °C/cm). These differences may be partially explained by substantial temperature attenuation due to turbulent mixing as well as the dependence of temperature data on the relative location of the probe strut within the fireball perimeter. As shown by the normalized intensity data in figure 9, the r.m.s. temperature intensities for the fireball wake are large and become comparable to mean-temperature levels, whereas core intensities are relatively small. Apparently, for these early fireball times, penetration of entrained ambient air into the fireball core region was limited as compared with the substantial mixing experienced by the fireball wake. Additional review of the temperature time-trace histories is consistent with this viewpoint.

3.6. *Turbulent structure statistics*

Statistical processing of the present temperature data was performed on selected segments of instantaneous temperature data as well as on validated wake data which had been redigitized into the locally stationary form (Bendat & Piersol 1971). These latter 'adjusted' data were obtained by subtracting the linear decay trend for the mean temperature from the instantaneous ('raw') temperature data. Based on these 'trend-removed' data, the sections that follow present such computed statistics as

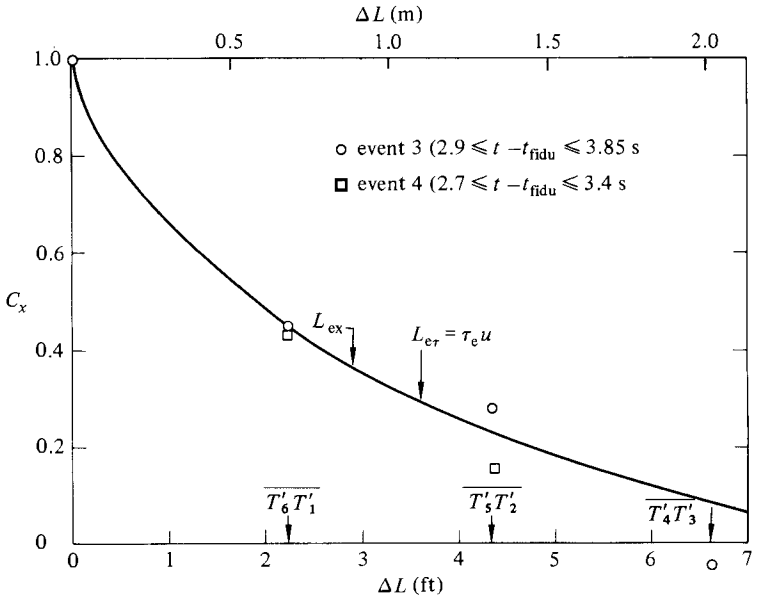

FIGURE 10. Temperature cross-correlation coefficient as a function of vertical probe separation.

auto- and cross-correlations, histograms (p.d.f.), skewness and flatness factors and power spectra densities (p.s.d.). Integral lengthscales, as well as eddy lifetimes based on moving-frame autocorrelation results, are also presented.

3.6.1. *Space/time correlation measurements*

Figure 10 summarizes spatial correlation data as measured by vertically aligned probes. The noted data, which show the variation of the cross-correlation coefficient with probe separation,

$$c_{xT} = \frac{\overline{T'(0,t)\,T'(\Delta x,t)}}{[T'(0,t)^2\,T(\Delta x,t)^2]^{\frac{1}{2}}}, \tag{4}$$

illustrate that the integral scale for the GEST fireball is of the order of three feet ($L_{ex} \approx 0.9$ m) based on an e-folding distance definition. Since turbulence investigators often estimate integral scales by transforming the autocorrelation timescale to a lengthscale through the local convective velocity ($L_{e\tau} = \tau u$), this lengthscale is also noted on figure 10, and it is seen to be about 20 % larger than the spatial scale. Such a result is consistent, however, with other turbulent flows that are similarly 'non-frozen' and where Taylor's hypothesis is expected to be only a rough approximation at best. The autocorrelation times used in this timescale calculation were based on averaging autocorrelation data for eight channels on event 3 and five channels on event 4. Combined results provide a correlation time of 41 ms, which converts to a spatial scale of $L_{ex} = 1.07$ m when transformed by the average wake convection velocity $u \approx 25.9$ m/s. All results shown in figure 10 are based on locally stationary data, an averaging time span of 0.6–0.7 s and correspond to fireball wake conditions at $t - t_{fidu} = 3.2$ and 3.0 s for events 3 and 4 respectively. Probe-separation distances are also shown on figure 10, and illustrate that the data as measured amply span the required scale dimensions. Using the fireball radius data from Bigoni & Matuska (1974), a normalized integral scale of

$$\frac{L_{ex}}{R_{FB}} \approx 0.054$$

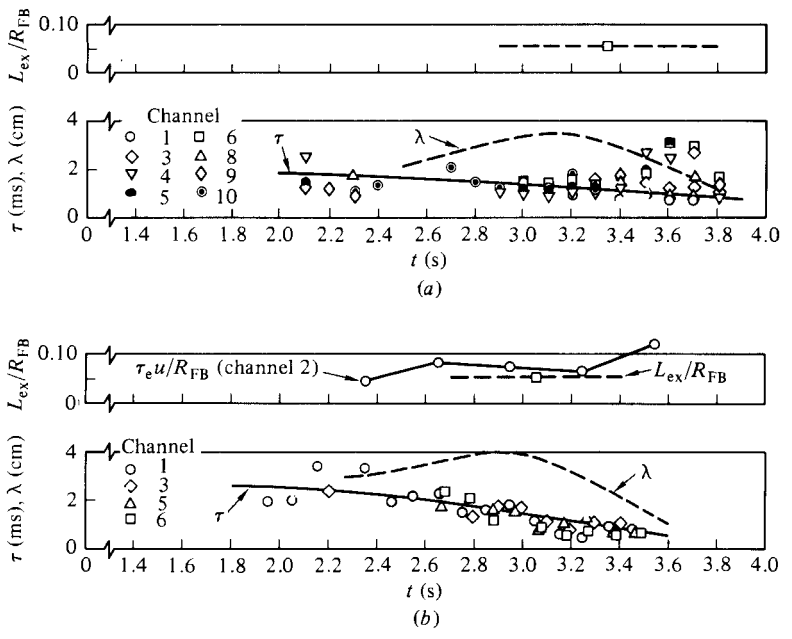

FIGURE 11. Summarized fireball scale data: (*a*) event 3; (*b*) event 4.

is calculated (figure 11). In addition to summarized velocity and temperature results, figure 11(*b*) also presents normalized scale data for channel 2 of event 4 based on measured autocorrelation times and mean-velocity data. Again, the transformed timescale, although comparable, is seen to be somewhat larger than the measured spatial scale.

Moving frame autocorrelation results for the current data base are shown in figure 12. These data typically provide a measure of eddy lifetime for a given turbulent flow. This timescale quantifies the decay (breakdown) behaviour of the large eddies and is approximately $\bar{\tau}_e = 0.17 \pm 0.04$ s. The ratio of moving frame to autocorrelation timescales (≈ 4) is comparable to results corresponding to data for other turbulent flows (≈ 2–5) and indicates that the intensities and gradients associated with the present buoyant thermals exhibit a highly persistent nature.

3.6.2. *Probability density distributions*

Figures 13(*a*, *b*) show summarized histogram results for events 3 and 4. The noted probability density distributions (p.d.f.) are seen to be 'spiky' in nature, with some evidence of bimodal behaviour. Ensemble-averaged skewness ($\sigma_3 = \overline{T'^3}/(\overline{T'^2})^{\frac{3}{2}}$) and flatness ($\sigma_r = \overline{T'^4}/(\overline{T'^2})^2$) factors for these events were $+0.1805/2.677$ and $+0.0308/2.697$ respectively. Note that for a Gaussian p.d.f. the skewness is zero and the flatness factor is 3. In general, the histogram data of figure 13 are seen to be skewed to the negative side of their normalized values. These non-Gaussian histograms are representative of the extent to which the GEST fireballs approximate a homogeneous turbulent temperature field, and thus provide a means to evaluate inherent uncertainties introduced by assuming a Gaussian probability density distribution in the fluid-mechanical and/or chemical model for a turbulent fireball.

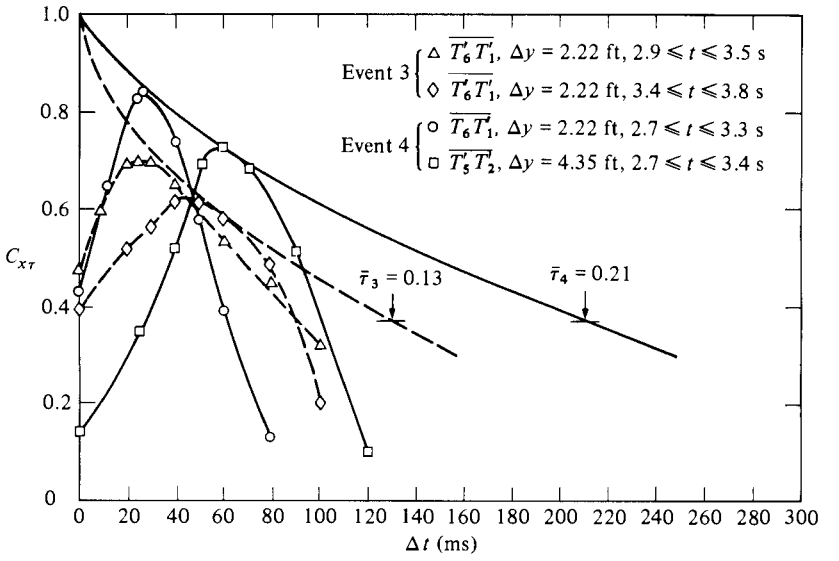

FIGURE 12. Moving-frame autocorrelation coefficient for temperature data ($2.7 \leqslant t \leqslant 3.4$ s).

3.6.3. *Temperature spectra*

A summary of temperature spectra data obtained under the current study is presented in figure 14. The data, as shown, are plotted as a function of normalized frequency, $n\tau$, where n corresponds to frequency and τ represents the measured autocorrelation time for a given channel. Also presented, as coabscissa, is the normalized wavenumber given by $kL = 2\pi n\tau$. Since the wavenumber is typically defined by $k = 2\pi n/u$, the integral lengthscale L is approximated in the present formulation by Taylor's hypothesis, i.e. $L = u\tau$. The data of figures 14(a, b) correspond to fireball 'wake' results as digitized and with the mean-temperature 'trend' removed.

In general, the results of figure 14 illustrate that the GEST temperature spectra follow approximately a $(n\tau)^{-\frac{5}{3}}$ falloff behaviour. Shown also on figure 14 is the familiar spectral distribution curve given by

$$\frac{E(n)}{E(0)} = \frac{1}{1+(2\pi)^2\,(n\tau)^2}. \tag{5}$$

Although this theoretical curve often compares favourably with spectral data for small-scale turbulent flows, it is seen here to fall off more rapidly than measured results. The favourable comparison of the present spectral data with Kolmogoroff's $-\frac{5}{3}$ law over several decades of spectral power illustrates that the 'spread' in the inertial subrange is large and that the data are consistent with the large turbulence Reynolds number for the GEST fireballs.

In an attempt to determine the dependence of spectral power on fireball location, the temperature results for channel 2 of event 4 were processed in data segments of $\Delta t = 0.3$ s for times from detonation ranging from 1.74 to 3.61 s (figure 14(c)). Note that these times span the fireball dimensions from the leading to the trailing edges. Although the data in general correspond more to a $(n\tau)^{-2}$ than $(n\tau)^{-\frac{5}{3}}$ falloff behaviour, it should be recognized that the frequency response for channel 2 (constant-*current* resistance thermometer, f_c = 1 kHz) was not as high as for the other

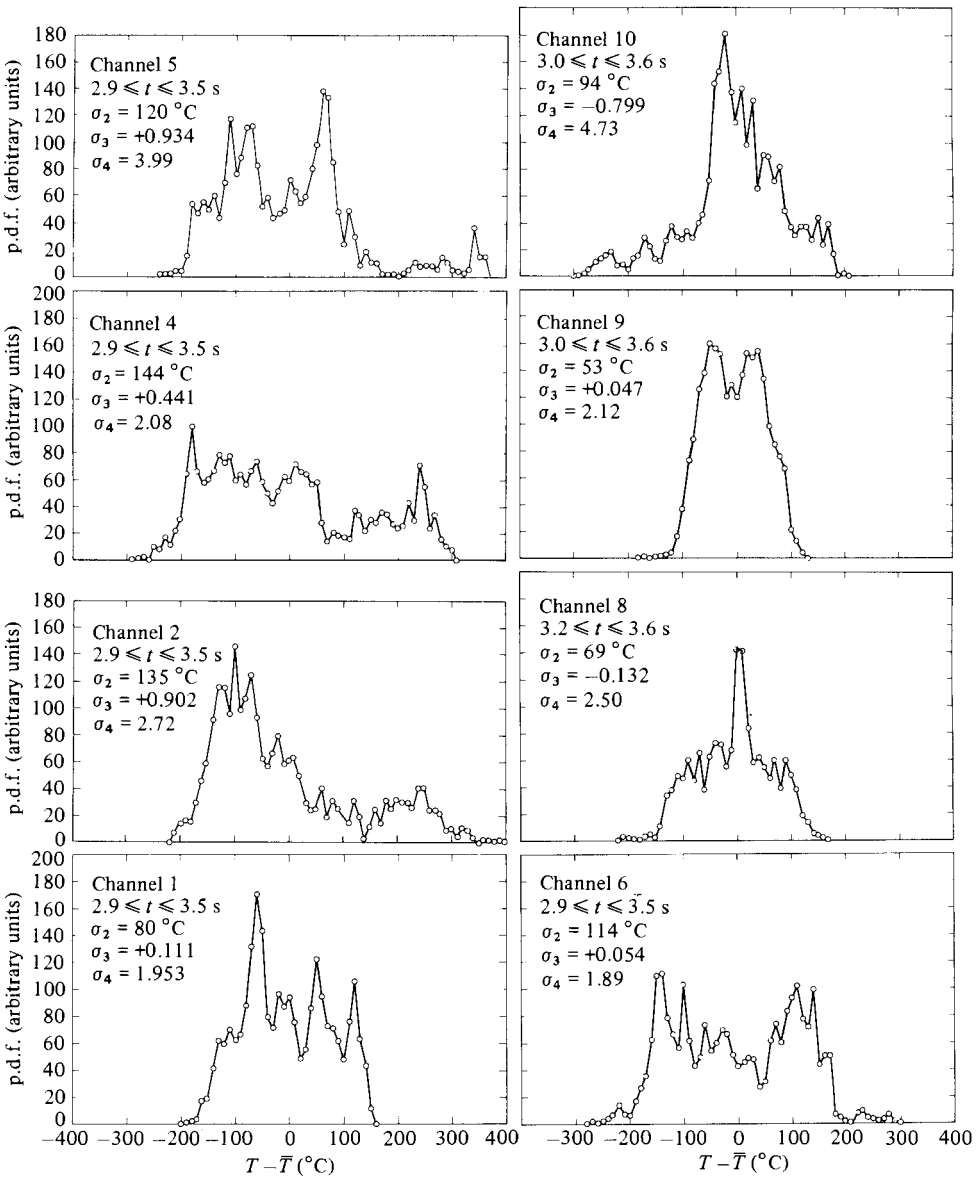

(*a*)

FIGURE 13(*a*). For caption see facing page.

channels (constant-*temperature* hot wire, $f_c = 5$ kHz) and therefore a somewhat faster falloff due to frequency response limitations was expected for the channel 2 results. Note, for example, that the channel 2 data in figures 14(*a*, *b*) also consistently fall off faster than results for the other channels. Except for the time slice 2.44–2.74 s, all spectral results in figure 14(*c*), including the one data segment corresponding to the complete set of fireball temperature data for event 4 (1.47–3.61 s), are seen to compare favourably. This latter result, as well as the spectral data presented in figures 14(*a*, *b*), illustrates that the turbulent spectral energy for the GEST fireballs is in general distributed in a well-behaved/nominal manner over all wavenumbers. On the other hand, the event 4 time segment for 2.44 s $\leqslant t \leqslant$ 2.74 s indicates that midfireball or core regions may

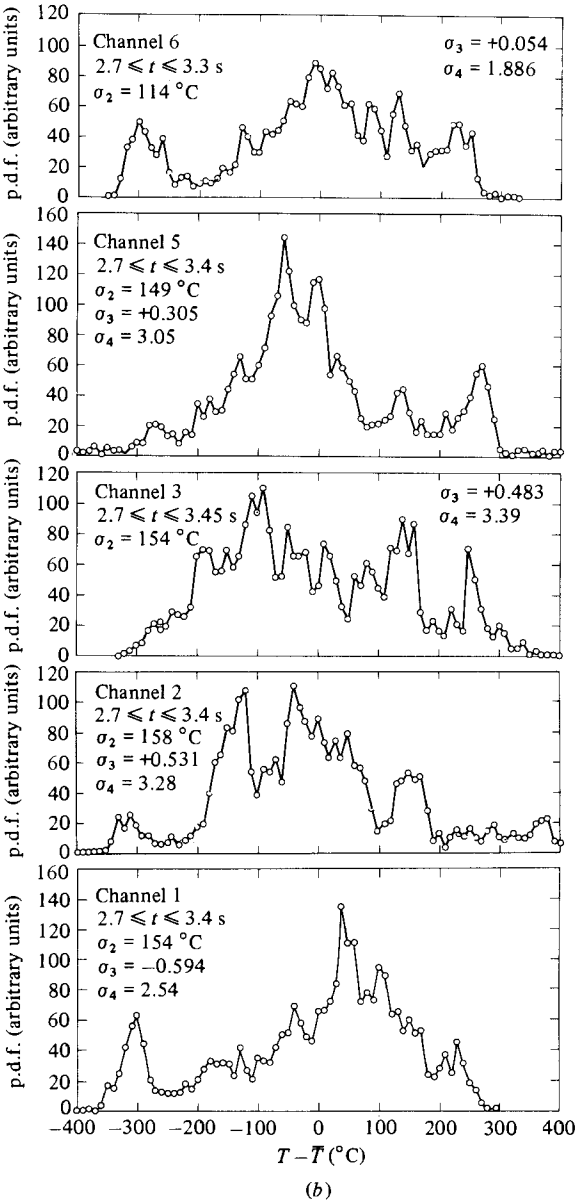

FIGURE 13. Probability density distributions for temperature fluctuations: (*a*) event 3; (*b*) event 4.

experience detectable energy enhancement at large wavenumbers (high frequency). This finding suggests that the small high-frequency eddies contained within the fireball core play a relatively more dominant role in this region's fluctuation energy content than that experienced in other parts of the fireball.

3.6.4. *Microscale data*

In isotropic turbulence the Taylor microscale for temperature fluctuations is given by

$$\overline{\left(\frac{\mathrm{d}T}{\mathrm{d}t}\right)'^2} = \frac{\overline{2T'^2}}{\tau^2}. \tag{6}$$

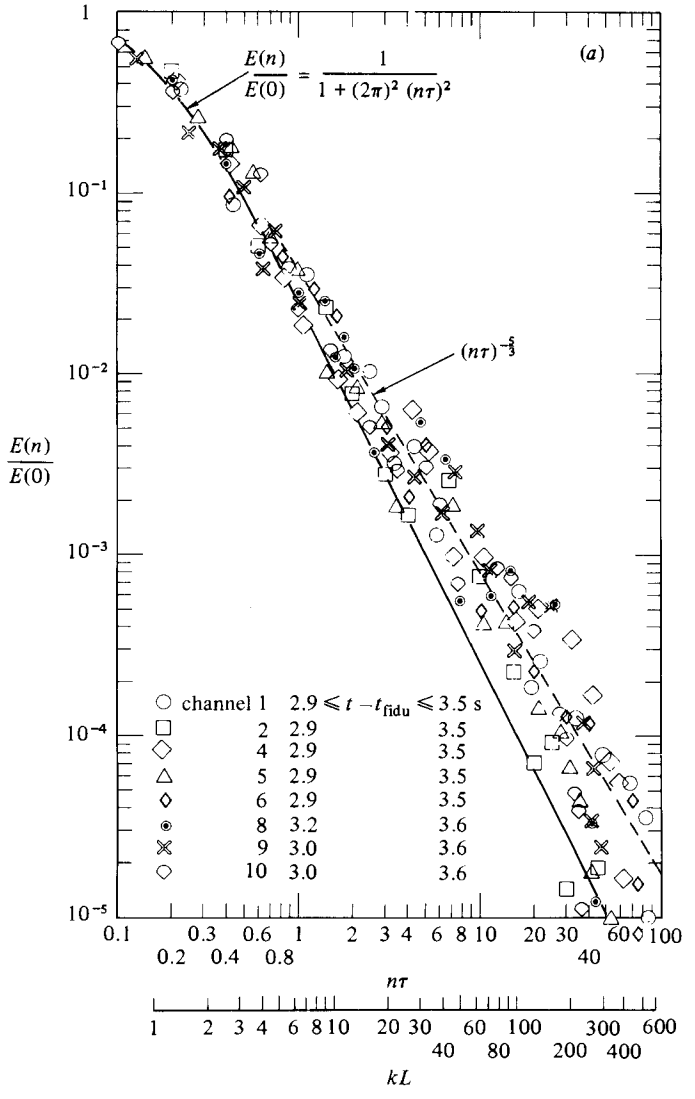

FIGURE 14(*a*). For caption see p. 24.

Based on this microscale formulation, the present digitized temperature data have been processed to provide approximate microscale data, as averaged and spatially transformed by the local velocity, for the GEST fireballs. Results (within a factor of two) suggest that time microscales vary from 1 to 3 ms (figure 11). As shown in figure 11, corresponding spatial microscales, determined by the local velocity transformation, vary between 2 and 4 cm. Because of the sensitive dependence of the temperature time derivative $[\overline{(\mathrm{d}T/\mathrm{d}t)'^2}]$ to signal-to-noise effects, some microscale results were also computed by subtracting the random-noise contributions (measured by non-fireball data) from the calculated raw data intensities. It was found that corrected scale data were at most only 20 % larger than uncorrected results.

Microscale values can also be estimated directly from isotropic turbulence theory (Tennekes & Lumley 1972; Hinze 1959), which provides the following microscale definition:

$$l = (15)^{\frac{1}{2}} l \left(\frac{\tilde{u}l}{\nu}\right)^{-\frac{1}{2}}. \tag{7}$$

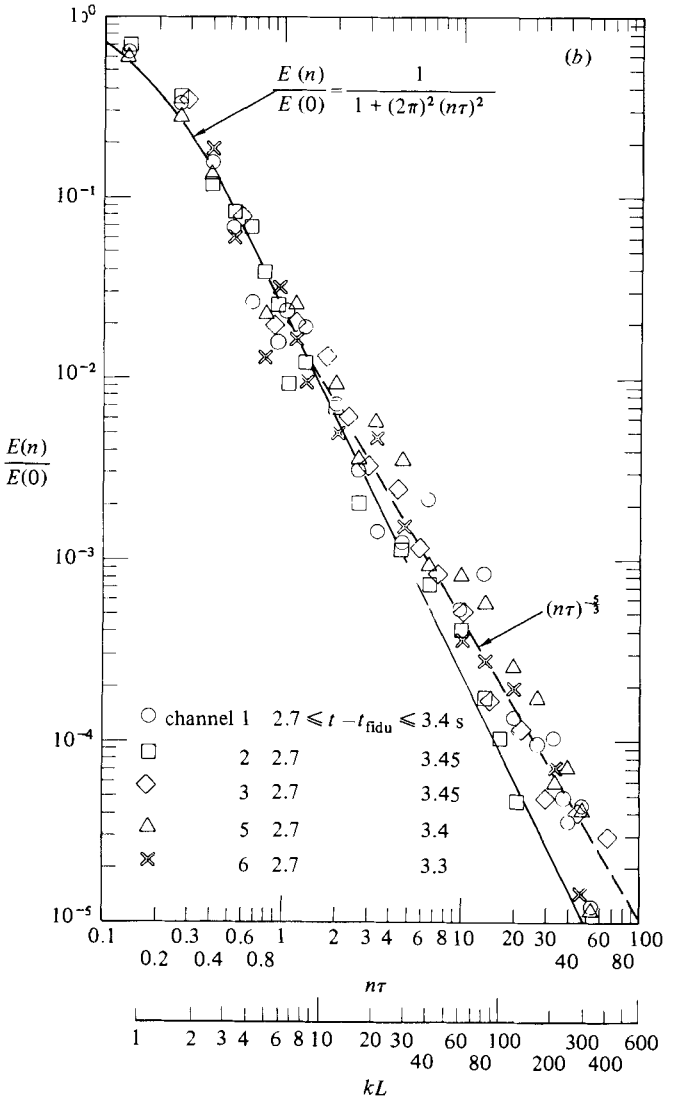

FIGURE 14(*b*). For caption see p. 24.

In (7), l represents the integral scale of turbulence, $\tilde{u}$ is the r.m.s. level for velocity fluctuations, and ν corresponds to the local kinematic viscosity. By assuming that the velocity intensity $\tilde{u}/\bar{u}$ is comparable to temperature intensity $\tilde{T}/\bar{T} \approx 0.2$, and, using measured temperature data to determine the viscosity and lengthscales, a predicted microscale of about 3.2 cm is calculated for events 3 and 4, corresponding to fiducial times of 3.2 and 2.7 s respectively. Not only is this predicted result in fair agreement with measured scale data (3.6 cm, figure 11), but measured trends generally behave in a consistent manner with the expected microscale dependence (7) on intensity, viscosity (temperature) and velocity between the core/wake interface and the fireball base. Since the turbulence Reynolds number

$$Re_\lambda = \frac{\tilde{u}\lambda}{\nu} \tag{8}$$

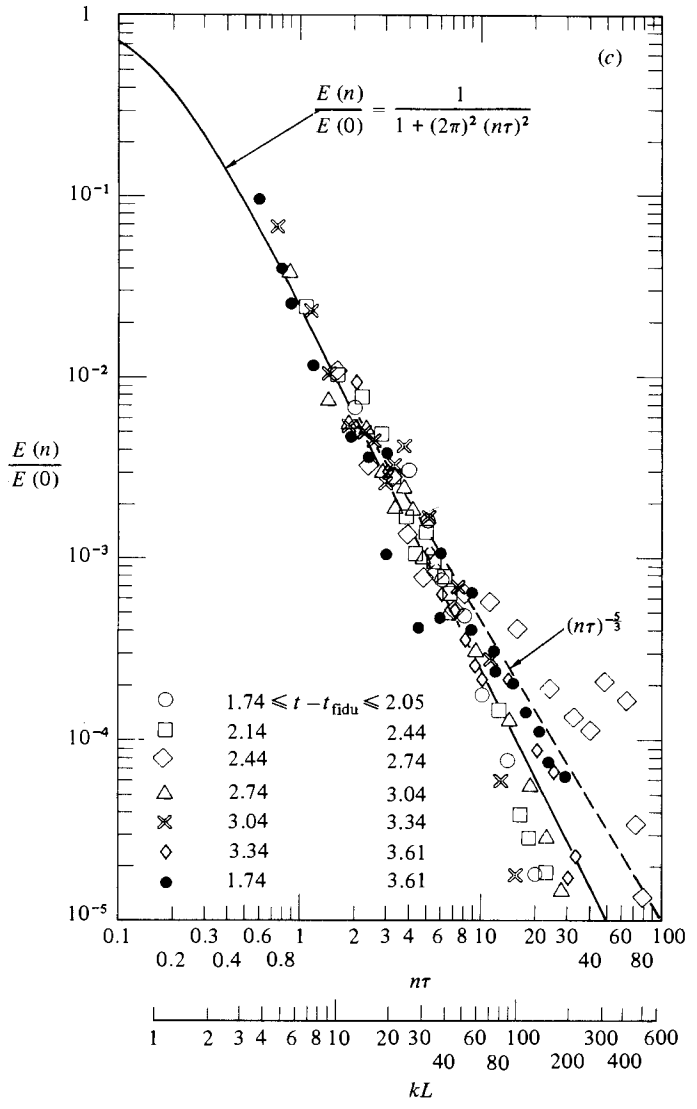

FIGURE 14. Normalized power-spectra for temperature fluctuations: (*a*) event 3 wake; (*b*) event 4 wake; (*c*) event 4 (channel 2).

for $\lambda = 2$ cm is about 2000 for the current results, the ratio of the Taylor microscale to the dissipation or Kolmogorov microscale, given by

$$\frac{\lambda}{\eta} = 15^{\frac{1}{4}} R_\lambda^{\frac{1}{2}}, \tag{9}$$

is approximately 90. It should also be noted that the indicated magnitude for the turbulence Reynolds number is 'large', and suggests that spectral results should display an inertial subrange $(n\tau)^{-\frac{5}{3}}$ covering several decades in spectral power. The AFWL spectral data discussed by Bigoni & Matuska (1974), as well as the TRW data of §3.6.3, indeed confirm that the $\frac{5}{3}$ behaviour holds true over a substantial range in wavenumber, and thereby further substantiate the well-developed turbulent nature of the early-time GEST fireballs.

4. Conclusions

Review of the present buoyant thermal temperature results illustrate that the early-time rising fireball is characterized by a highly intermittent irregular fireball top or cap, a constant (high-) temperature core and a thermal wake exhibiting a linear decay in mean temperature. Not only are temperature fluctuations near the fireball 'top' and bottom of the same order as local mean temperatures, but these fluctuations as well as temperature and temperature gradients are all higher at the leading edge of the fireball as compared with corresponding values at the trailing edge. This is evident, for example, in the 'sudden' growth in temperature/intensity at the top of the fireball as compared with the gradual decay at the fireball base. Leading edges of 'hot' eddies and the fireball core are generally characterized by steep temperature gradients relative to trailing edges which contain relatively shallow gradients. Hot fluid motion at the fireball top consists of steep-gradient large-scale structure in combination with random pockets of intense turbulent activity. The presence of ambient air eddies embedded/entrained within the fireball top and wake is evident in the temperature history data as well as in available GEST photographic results. This approximate thermal 'picture' of rising buoyant thermal is based on the quantitative results presented herein and agrees favourably with available laboratory data for buoyant thermals.

This work was sponsored by the Defense Nuclear Agency and was monitored by the Air Force Weapons Laboratory, Air Force Systems Command, under Contract DNA 001-74-C-0067.

REFERENCES

BATT, R. G. 1976 Hot wire measurements of temperature field structure within GEST fireballs. *DNA* 3936T.

BENDAT, J. S. & PIERSOL, A. G. 1971 *Random Data: Analysis and Measurement Procedures.* Wiley Interscience.

BIGONI, R. A. & MATUSKA, D. A. 1974 Preliminary report on project gas explosive simulation technique. *AFWL* TR-74-252.

BLACKMAN, R. G. & TUKEY, J. W. 1958 *The Measurement of Power Spectra.* Dover.

BRADSHAW, P. 1971 *An Introduction to Turbulence and Its Measurement.* Pergamon.

CORRSIN, S. 1949 Extended applications of the hot-wire anemometer. *NACA TN* 1964.

HINZE, J. O. 1959 *Turbulence.* McGraw-Hill.

KOVASZNAY, L. S. G. 1954 Turbulence measurements – hot wire method. In *Physical Measurements in Gas Dynamics and Combustion*, pp. 213–276. Princeton University Press.

KNAPP, W. S. & SCHWARTZ, L. 1975 Aids for the study of electromagnetic blackout. *DNA* 3499H.

LAMB, H. 1932 *Hydrodynamics*, 6th edn. Dover.

LIN, S. C., TSANG, T. & WANG, C. P. 1972 Temperature field structure in strongly heated buoyant thermals. *Phys. Fluids* **15**, 2118.

MANTROM, D. W. & HAIGH, W. W. 1974 Fireball entrainment study. *DNA* 3248F.

SCORER, R. S. 1957 Experiments on convection of isolated masses of buoyant fluid. *J. Fluid Mech.* **2**, 583.

TAYLOR, G. I. 1950 The formation of a blast wave by a very intense explosion. II. The atomic explosion of 1945. *Proc. R. Soc. Lond.* A **201**, 175.

TSANG, L. C. H. 1974 Initial formation geometry and evolution of temperature field in buoyant thermals. MSE thesis, University of California, San Diego.

TENNEKES, H. & LUMLEY, J. L. 1972 *A First Course in Turbulence.* MIT Press.

WOODWARD, B. 1959 The motion in and around isolated thermals. *Q. J.R. Meteor. Soc.* **85**, 44.